AAS 16-538

RESIDENT SPACE OBJECT DETECTION USING ARCHIVAL THEMIS FLUXGATE MAGNETOMETER DATA

Julian Brew[*], Marcus J. Holzinger[†]

Although the detection of space objects is generally achieved using optical and radar measurements, these methods are limited in the capability of detecting small space objects at geosynchronous altitudes. This paper examines the use of magnetometers to detect space objects by introducing a matched filter scoring approach and evaluating it using archival fluxgate magnetometer data from the NASA THEMIS mission. Relevant data-set processing and reduction is discussed in detail. Supporting evidence for using magnetometers to detect resident space objects is presented. Plausible detections of charged space objects are reviewed.

INTRODUCTION

As highlighted in the 2010 U.S. National Space Policy, the growing space debris problem is creating a major challenge for Space Situational Awareness (SSA) and the safe operation of U.S. space assets.[1] The objective of Space Situational Awareness is to detect, characterize, and track space objects (SO). Although the U.S. Space Surveillance Network (SSN) currently tracks 22,000 space objects with diameters greater than 10 cm,[2] additional optical and radar data indicate that there are approximately 500,000 objects larger than 1 cm and more than 100 million larger than 1 mm in the space environment.[3] Because of the high impact speed between objects in Earth orbit, small debris (less than 1 mm), can pose a threat to current and future operational U.S. space assets and human spaceflight.

Presently, the SSN Space Object Catalog (SOC) uses optical and radar measurements as the primary method in the detection of space objects.[4] However, in geosynchronous (GEO) orbits, where a large number of communications and weather spacecraft are located, optical and radar methods struggle at detecting small, faint objects. With the accumulation of small debris in GEO orbits due to defragmentations,[5] a method of detecting and characterizing small and poorly characterized space objects is needed.

One possible detection method that addresses these needs is measuring induced magnetic fields generated by charged space objects as they pass near a magnetometer. Due to interactions with solar wind in Earth's magnetic field, resident space objects (RSOs) in Earth orbit accumulate static Coulomb charges over time.[6] Because moving charged particles generate an electromagnetic field, magnetometers can in theory sense these phenomena and can be used to detect, track, and characterize charged space objects. This concept has been pursued in Low Earth Orbit (LEO) experiments

[*]Undergraduate Student, The Guggenheim School of Aerospace Engineering, Georgia Institute of Technology, Atlanta, GA 30332, AIAA Student Member

[†]Assistant Professor, The Guggenheim School of Aerospace Engineering, Atlanta, GA 30332, AIAA Senior Member

such as Clementine (orbital meteoroid and debris counter),[7] although to limited effect. These experiments used capacitor detectors that sensed magnetic field fluctuations above a specified threshold which resulted in statistical space debris representations. This differs from a magnetometer detection as it provides a sequence of three axis magnetic field measurements as a function of time for each RSO encounter.

There are a number of observable and unobservable parameters for encounters between a charged RSO and a three axis magnetometer. Previous investigations have shown the orientations of the charged object flyby and the closest approach distance cannot be determined with the given magnetic encounter information.[8] However, constraints based on the RSO orbit energy, periapsis radius, Coulomb charge, and the detection range of the sensing magnetometer can be imposed to identify admissible regions for initial orbit determination efforts.[9]

Matched filters are formed by correlating a known template signal with the unknown signal to detect the presence of the known signal in the unknown signal.[10] With additive stochastic noise, matched filters maximize the signal to noise ratio (SNR) gain.[11] Using the Biot-Savart law,[12] induced magnetic field template signals can be generated that depend on the relative motion between the magnetometer and the space object. These template signals can be used in conjunction with matched filters to detect the presence of a magnetic field signature characteristic of a charged RSO flyby in experimental data. In this paper, the matched filters are applied to fluxgate magnetometer data acquired from the NASA "Time History of Events and Macroscale Interactions during Substorms" (THEMIS) mission.[13,14]

Matched filters perform convolutions between the known template signal and the unknown signal.[11] While a time convolution is usually the correlation method used in matched filters, a different variation of the matched filter using Pearson product-moment correlation coefficient[15] is presented in this paper. In this paper, a matched filter scoring method is introduced and shown to approximate the SNR of the magnetic field fluctuation due to the charged RSO flyby.

The expected contributions from this research include: 1) The generation of Matched Filter template hypotheses is described 2) A signal detection hypothesis test framework is developed and explained and 3) An examination of on-orbit THEMIS data is performed to investigate the plausibility of RSO detection using magnetometer hypothesis.

THEORY

Expected Magnetic Signatures of RSO Flyby

Earth orbiting objects interact with the space plasma environment, resulting in the accumulation and transport of electric charge. Because of this, spacecraft and space objects can acquire a static Coulomb charge over time. Low altitude orbiting spacecraft (LEO) usually experience less charging effects than at high altitude (GEO), where the spacecraft encounter high-energy, low-density electrons.[16] Freuh et al. used numerical simulation of the magnetic field and solar wind activity to estimate the Coulomb charges of space debris material, in particular mylar and kapton. For these materials, the total charge can range from -0.003 to -0.115 Coulombs in GEO depending on solar weather and material capacitance.[17]

For charged RSO encounters, an approximate flyby motion model was derived by Holzinger.[8] In the flyby motion model, the local relative motion is approximately linear over the ranges at which the magnetic field can be detected. From the Biot-Savart law, the magnetic field $\boldsymbol{B}(t)$ sensed at

the magnetometer location and generated by a moving object with sensed charge q_s (Coulombs), relative velocity $\dot{\boldsymbol{\rho}}$, and relative position $\boldsymbol{\rho}$ is

$$\boldsymbol{B}(t) = (\tfrac{\mu_0 q_s}{4\pi})\frac{\dot{\boldsymbol{\rho}}(t)\times\boldsymbol{\rho}(t)}{\|\boldsymbol{\rho}(t)\|^3} \tag{1}$$

where $\boldsymbol{B}(t)$ is in units of Teslas, $\mu_0 = 4\pi \times 10^{-7}$ Vs/Am is the magnetic permeability, $\dot{\boldsymbol{\rho}}(t)$ has units of meters per second, and $\boldsymbol{\rho}(t)$ has units of meters. Rewriting Eq. (1) with assumed relative motion model, the final observable measurement equation for a magnetometer with a moving charged particle can be written as

$$\boldsymbol{B}(t) = -(\tfrac{\mu_0}{4\pi})\frac{\mathcal{Q}_s\omega_m}{(1+\omega_m^2(t-t_c)^2)^{\frac{3}{2}}}\hat{\boldsymbol{p}}(\alpha,\beta) \tag{2}$$

where t_c is the time of closest approach and $\hat{\boldsymbol{p}}(\alpha,\beta) = \boldsymbol{\rho}\times\dot{\boldsymbol{\rho}}/\|\boldsymbol{\rho}\times\dot{\boldsymbol{\rho}}\|$ is the unit vector that defines the plane of motion of the encounter parametrized in polar coordinates α and β. Both the distance normalized apparent charge parameter, $\mathcal{Q}_s = q_s/\rho_\perp$, and the maximum apparent angular rate $\omega_m = \|\dot{\boldsymbol{\rho}}\|/\rho_\perp$ have been normalized by the closest approach distance of the RSO to the magnetometer $\rho_\perp$. From this, there is an unobservable two-dimensional subspace with respect to $\rho_\perp$ and the orientation of the flyby in the encounter plane. For signature detection, however, it is only necessary to examine $\|\boldsymbol{B}(t)\|$. This reduces the number of unobservable parameters to one, $\rho_\perp$.

Depending on the sampling rate and corresponding Nyquist frequency of the sensing magnetometer, there are inherent limitations on the relative RSO speeds that the magnetometer can accurately detect. Conversely, depending on the expected relative speeds between the magnetometer and the RSO, there may be a limitation on the required magnetometer sampling rate to capture the RSO encounter.

Holzinger discussed the effect of charge screening and local space weather on the sensed magnetic field.[8] Due to the interaction between an orbiting object and the space plasma environment, the sensed charge of an object is reduced. Consequently, the sensed magnetic field due to this charge is also weakened. The Debye length, denoted by λ_d, is the characteristic distance parameter that describes the exponential decay of charge screening. At GEO altitudes, the effective Debye lengths of plasma are on the scale of 4 -1000 m enabling the detection of charged objects on the order of meters to hundreds of meters.[6]

For the charged object to be detected by the magnetometer and distinguished amongst local variations in the magnetic field, the SNR of the induced magnetic field Eq. (2) must exceed a set threshold. Using this, the following detection constraint in Eq. (3) for a RSO detection using a magnetometer is created.[8]

$$\rho_\perp^2 e^{\frac{\rho_\perp}{\bar{\lambda}_d}}\sigma SNR_{det} \leq (\tfrac{\mu_0|q_v|}{4\pi})\|\dot{\boldsymbol{\rho}}\| \tag{3}$$

The bounds of this inequality can be found analytically.

$$\rho_{\perp,max} = 2\bar{\lambda}_d W(\frac{\sqrt{\frac{\mu_0}{4\pi}|q_v|\|\dot{\boldsymbol{\rho}}\|}}{2\bar{\lambda}_d\sqrt{\sigma SNR_{det}}}) \tag{4}$$

W is Lambert W (also known as the product logarithm) function[18] and is the analytical solution to $f(x) = xe^x$. Eqn. (4) gives the maximum closest approach distance for a magnetometer RSO

detection as a function of the vacuum charge of the RSO (q_v), the relative velocity of the RSO to the magnetometer ($\|\dot{\boldsymbol{\rho}}\|$), the local space weather conditions given with the effective Debye length ($\bar{\lambda}_d$), and the measurement precision of the magnetometer (σ). For example, Figure 1 displays the RSO detection capability of the THEMIS fluxgate magnetometers at GEO altitudes and various effective Debye lengths. Stiles et al. computed the effective Debye lengths using the Debye-Huckel approximation during low, nominal, and high levels of solar activity.[6]

Under the best-case conditions of space weather and charge, the THEMIS fluxgate magnetometers are able to detect RSO flyby signatures at a distance of about 650 m. It should be noted that this upper limit depends on the relative speed between the magnetometer and the charged objects. The THEMIS fluxgate magnetometers in consideration are capable of a sampling rate of 128 Hz. At this rate, the magnetometers can measure sufficient samples to capture RSO flyby encounters with relative speeds of about 2400 m/s. Although this speed is relatively large for GEO altitude encounters, the maximum detection distance described in Eqn. (4) scales logarithmically with relative speed. For example, above 500 m/s, a decrease in the relative speed by a factor of two results in about an 11% decrease in the detection range defined by $\rho_\perp$.

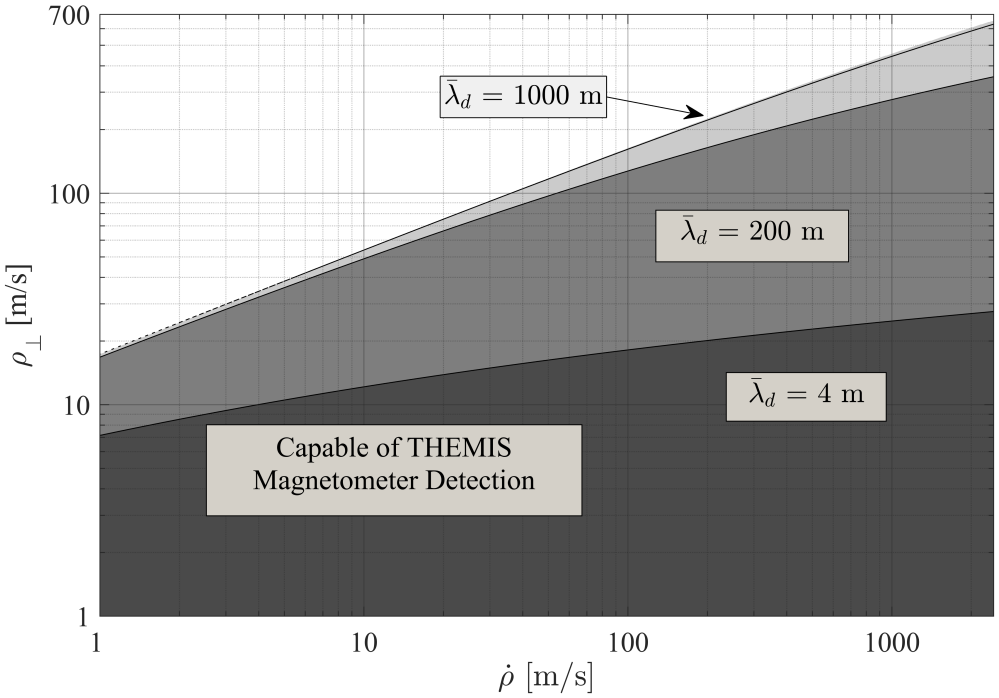

Figure 1. Detection Capability of THEMIS Magnetometer at Various Space Weather Conditions

Potential Magnetosphere Phenomenon

Magnetosphere phenomenon are of particular importance to the detection of RSOs through magnetometer flybys. Depending on the frequency and magnitude of the extraneous magnetic field variations, it becomes more difficult to detect low SNR RSO signatures and to distinguish between the RSO signatures with local variations in the magnetic field. Furthermore, local magnetosphere phenomenon are time-varying and difficult to predict. Therefore, signal conditioning is required

in the process of detecting charged RSO encounters to attenuate the signals due to magnetosphere phenomenon.

The magnetosphere is the boundary that separates Earth's magnetic field and the solar wind. Inside of the magnetosphere the varying conditions, typically referred to as space weather, greatly depend on the solar activity. The interaction between the solar wind and the magnetosphere creates phenomena such as the bow shock, magnetopause, magnetotail, magnetic field reconfigurations, and geomagnetic storms.[19]

The main magnetic field of the Earth is slowly varying and originates within the Earth. However, more rapid variations, with periods from seconds to days, are produced by the interaction between Earth's magnetic field and the Sun's radiation.[20] For example, there are two primary effects of the Sun due to it's position relative to the Earth - quiet day magnetic variations and magnetic storms.

A quiet day magnetic variation originates from the Sun's electromagnetic and thermal radiation. As the day side of the Earth is illuminated and heated, the Sun's radiation heats the ionosphere causing convection. The convection moves charged particles through the Earth's magnetic field which itself produces a magnetic field that is fixed on the day side of the Earth. The axial rotation of the Earth carries a site on the surface in and out of this magnetic field creating a 12-hour variation.[19] Magnetic storms, on the other hand, are a product of the Sun's ejection of solar wind. Coronal mas ejections from the Sun's surface further compress the magnetosphere causing a sudden change in the magnetic field. At GEO altitudes, it can be shown that the local magnetic field variation is positively proportional to variations in solar wind dynamic pressure.[21] Because solar wind dynamic pressure is variable and unpredictable in time, the resulting magnetic field fluctuations are similar.

Another phenomenon of interest is geomagnetic pulsations, which are plasma waves in the Earth's magnetosphere that can range from about 0.0016-10 Hz.[22] The higher frequency waves are proton ion-cyclotron waves in the magnetospheric plasma and can reach amplitudes of a few nanotesla.[22] An example of these pulsations in the THEMIS-D data can be seen in Figure 2. At the higher frequencies, these pulsations can significantly alter the frequency content of the local magnetic field.

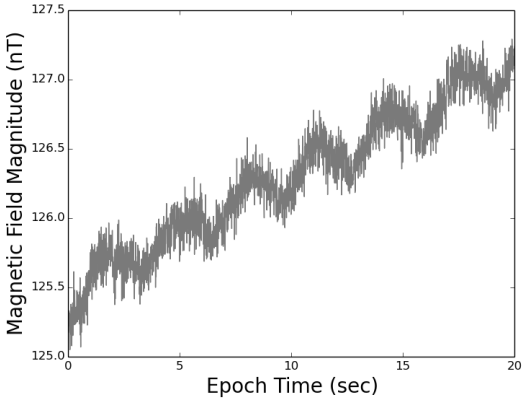

Figure 2. Geomagnetic Pulsations in THEMIS-D Data with Epoch Time of Wednesday, 09-Sep-15 07:04 UTC

Signal Conditioning

Only the induced magnetic field due to a RSO flyby is desired in the matched filter scoring process. In general, the baseline magnetic field can be approximated using numerical Earth magnetic field models such as the IGRF and the WMM.[20] However, there are model uncertainties on the order of 150 nT[20] and significant spatial variations in the Earth's magnetic field.[23] Additionally, the variations in the local magnetic field due to space weather phenomena must also be attenuated as much as possible for the matched filter. Thus, the raw magnetometer data must be processed to locally approximate the baseline magnetic field. This can be achieved by using the relationship described in Eq. (5), where $r(s)$ is the residual signal, $d(s)$ is the raw signal, and $L(s)$ is a zero-phase low pass filter. This detrending and filter process is demonstrate in Figure 3. In this particular example, the cut-off frequency was set to demonstrate the capability of this approach to isolate magnetic field peaks at a given frequency. For this approach, the cut-off frequency of the low pass filter, ω_c, is a function of ω_m to ensure the correct frequencies are maintained and eliminated in each template function of the scoring process, shown in Eq. (6). The k constant is a tuning parameter set to 4π in this work. This choice in k ensures the cutoff frequency is both sufficiently below the ω_m of interest to avoid signal attenuation at that frequency. This results in isolating the zero-mean magnetic field signal that describes the local fluctuations at the frequency of interest.

$$r(s) = (1 - L(s, \omega_c))d(s) \tag{5}$$

$$\omega_c = \frac{\omega_m}{k} \tag{6}$$

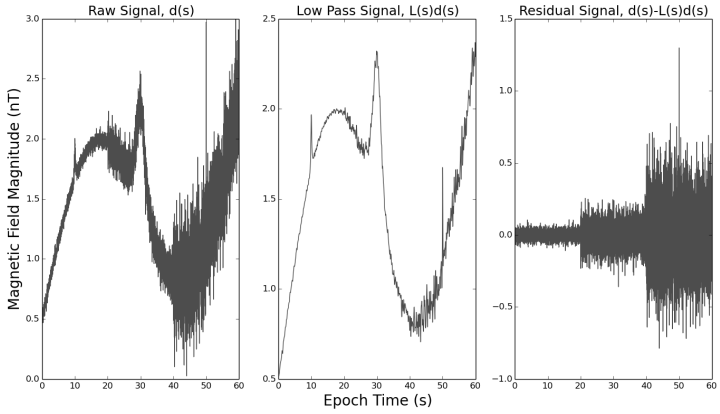

Figure 3. Demonstration of Low Pass Filtering Process on Artificial Signal

Matched Filtering

A template signal is created from the expected RSO flyby magnetic field signature described in Eq. (2). To avoid a template signal dependence on the charge q_s and the unobservable parameter $\rho_\perp$ the template signal used in the matched filters is shown in Eq. (7). Examples of the template signals with varied ω_m can be seen in Figure 4.

$$g(t, \omega_m) = \frac{\omega_m}{(1+\omega_m^2(t-t_c)^2)^{\frac{3}{2}}} = \frac{\|\boldsymbol{B}(t)\|}{(\frac{\mu_0}{4\pi})\mathcal{Q}_s} \tag{7}$$

The matched filters applied to the THEMIS magnetometer data use the Pearson product-moment correlation coefficient[15] when correlating the template signal and the magnetometer data signal. The correlation coefficient metric is used because of the frequency resolution in correlating unknown signals consisting of multiple frequencies with a template signal consisting of a single frequency. However, this metric results in correlations valued at or between -1 and +1 for an purely negative and positive correlation, respectively. To scale these results based on the magnitude of the magnetic field fluctuations, the acquired correlation coefficients are scaled by the local SNR of the magnetometer signal. The local SNR of the magnetometer signal is defined as

$$\text{SNR}(t) = \frac{\|\boldsymbol{B}(t)\|}{\sigma(t)} \tag{8}$$

where the magnetometer is assumed to have noise characterized by a zero-mean Gaussian and time varying standard deviation of $\sigma(t)$. Under this scaling metric defined in Eq. (8), the SNR of the RSO magnetic field signature is approached and low intensity magnetic field fluctuations do not affect the output of the matched filters. Note that the $B(t)$ described thus far is the induced magnetic field from the RSO flyby. This can be acquired by subtracting the baseline magnetic field from the raw magnetometer signal as displayed in Figure 3.

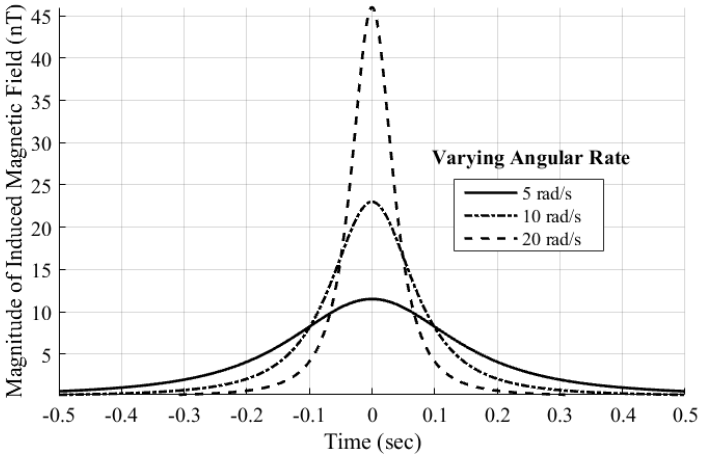

Figure 4. Example Template Signal with Varying Angular Rate (ω_m)

As previously mentioned, matched filters are formed by correlating template and data signals through time. However, the induced magnetic field from the RSO flyby drastically changes with the relative angular rate, ω_m. To effectively detect RSO encounters over a wide range of RSO angular rates, the matched filter described above is applied to the magnetometer data signal multiple times with varying ω_m. This scoring process, illustrated in Figure 5, is defined as the application of the matched filters over both time and RSO flyby angular rate. Now instead of a one-dimensional matched filter output signal, a scoring surface is generated as a function of time of closest approach and RSO maximum apparent angular rate.

By varying ω_m of each template signal in the scoring process, the time scale of the template signal is also being varied. If the scaling parameter $\alpha \in (0, 1)$ is defined, the time interval at which the peak of the induced magnetic field occurs can be quantified. Using the geometry described in Figure 6 and the magnetic signature described in Eq. (2), the time interval can be calculated as shown in

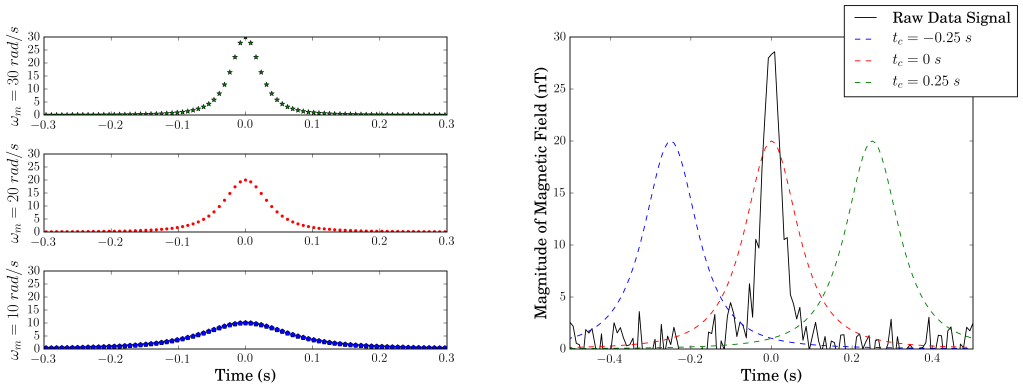

(a) Template Signals with Varying ω_m

(b) Template Signals with Varying t_c

Figure 5. Visualization of Scoring Process

Eq. (8). The approximate frequency of the RSO flyby can also be approximated.

$$\Delta t = 2\frac{\sqrt{\alpha^{-2/3}-1}}{\omega_m} \tag{9}$$

The set value of α can vary depending on the sampling rate of the magnetometer data and the range of ω_m used in the scoring process. For example, the minimum time interval may be defined such that there are a minimum of 5 samples measured. At a sampling rate of 128 Hz, this corresponds to a minimum time interval of about 39 milliseconds. An additional constraint on the maximum value of ω_m can be enforced by selecting lower and upper bounds for $\rho_\perp$ and $\dot{\rho}$, respectively. A conservative estimate of the minimum expected closest approach distance of $\rho_{\perp,min} = 25$ m is set. Due to the 128 Hz maximum sampling rate of the THEMIS fluxgate magnetometers, the largest relative speed that can be detected in a magnetic field signature is $\dot{\rho}_{max} = 2430$ m/s. With constraints on both parameters, the required $\alpha \approx 0.0166$. By keeping α fixed during the scoring process, a given ω_m maps to a unique template function. This α parameter also ensures equal weighting between matched filter results over multiple ω_m and corresponding template functions.

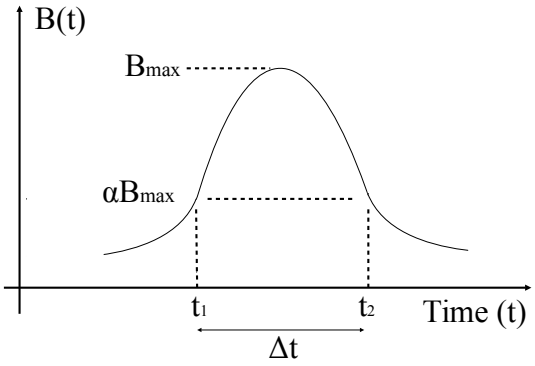

Figure 6. α Parameter Geometry

Due to the inclusion of the variable template function time intervals, at each ω_m of the scoring

process there will be a time delay between the true time at which a RSO flyby signature occurs and the maxima of the matched filter output. Therefore, to correctly identify the closest approach time (t_c), a time shift of $\Delta t/2$ must be added to the matched filter result. As a result of performing the matched filter over various ω_m, the time shift must be applied at each iteration of matched filter results. The results of this paper include this time shift.

EXPERIMENTAL DATA AND RESULTS

THEMIS Mission Description

The THEMIS mission, launched in 2007, studies magnetic substorms and the interactions in Earth's magnetosphere that influence them. The constellation maintained five spacecraft until spring 2011 when two of the spacecraft separated into a new NASA mission around the Moon. This new mission, "Acceleration, Reconnection, Turbulence and Electrodynamics of the Moons Interaction with the Sun" (ARTEMIS), measures the effect of the Sun's radiation the Moon.[24] To aid in the characterization of the magnetosphere and magnetic substorms, the THEMIS mission measures the local magnetic field using search-coil and fluxgate magnetometers. As shown in Figure 7(a), the THEMIS spacecraft were placed in highly elliptical orbits where the respective apogee rotate slowly around the Earth to survey the various sections (i.e. day-side, night-side, etc.) of the magnetosphere. After the departure of the two ARTEMIS spacecraft in early 2010, the remaining THEMIS spacecraft settled into a science orbit, displayed in Figure 7(b), to continue monitoring space weather phenomenon.

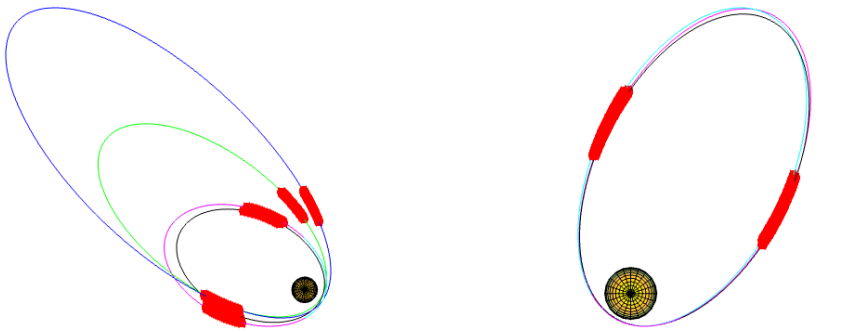

(a) Orbit Geometry 2007-2009 (b) Orbit Geometry 2010-Present

Figure 7. THEMIS Orbit Diagrams with Highlighted GEO Altitude Belt

To accomplish the mission's science goals, the THEMIS spacecraft incorporate high sampling rate on-board fluxgate magnetometers with 3-σ measurement uncertainties of 10 pT/$\sqrt{\text{Hz}}$ at 1 Hz.[13] At the magnetometers maximum sampling rate of 128 Hz, this corresponds to a 3-σ measurement uncertainty of 113 pT, which is on the order or lower than the magnitude of the potential magnetic signature from a RSO.

To measure the characteristics and behavior of magnetosphere phenomena, the science instruments on each THEMIS craft operate in one of four science collection modes: slow survey, fast survey, particle burst, and wave burst. For the majority of an orbit, the spacecraft operates in slow survey, returning electric, magnetic, and plasma parameters once every 3 seconds ($\frac{1}{3}$ Hz). Near

apogee in the magnetotail and regions of interest like the dayside (towards Sun) magnetopause, the spacecraft operates in fast survey mode, collecting data at 4 Hz. Additionally, encounters with the bow shock, magnetopause, high density plasma regions, geomagnetic storms, and other phenomena trigger burst mode operations, where the fluxgate magnetometer can sample the magnetic field at 128 Hz.[13]

Extraction and Processing of Data

In this study, only the GEO radius (35,000-50,000 km) orbital range is of interest, as highlighted in Figure 7. As such, the THEMIS fluxgate magnetometer datasets from only the GEO altitude range are processed in the matched filter scoring process. Due to Debye lengths on the centimeter to meter scale, charge screening severely limits detection ranges to less to 1 m at LEO altitude. At an orbit radius of 35,000 km, the Debye length reaches values at which space object detection using magnetometers is feasible. Orbit radii above 50,000 km were not considered as there is not a large population of space objects beyond the altitudes of GEO objects and the GEO disposal orbits.

In the aforementioned matched filter process, the data volume to access and analyze is large due to the high resolution data products supplied from each of the THEMIS spacecraft. As shown in Figure 8, the total amount of data to parse and analyze is about 450 GB.

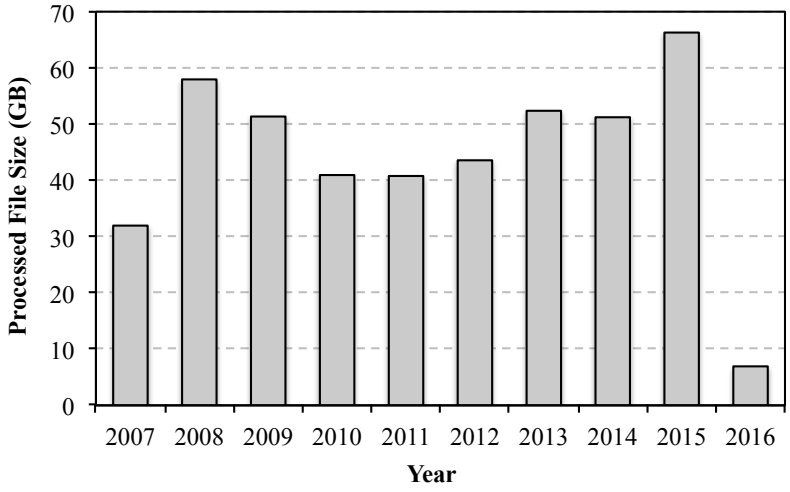

Figure 8. Total THEMIS Fluxgate Magnetometer Data Volume

The data capacity and computational requirements of this problem called for the use of the Partnership for an Advanced Computing Environment (PACE) high-performing computing clusters at the Georgia Institute of Technology. The PACE clusters are used for the acquisition of the fluxgate magnetometer data, parsing and constraining the data, as well as the computations involved in the matched filter scoring process to detect RSO encounters. Additionally, there are large benefits in computation speed provided by the capability to parallelize the computation processes across multiple nodes of the cluster.

Figure 9 summarizes the overall algorithm used to acquire and process the THEMIS magnetometer data. The first component of the process involves pulling the fluxgate magnetometer data from public NASA servers. The NASA Coordinated Data Analysis Web data service and the NASA

Space Physics Data Facility provide a publicly-released database directly accessible as an anonymous File Transfer Protocol (FTP) service. Once the magnetometer data is acquired in the form of a Common Data Format (CDF) file, the contents of this archived file are unpacked into the relevant data products such as spacecraft orbital state arrays, state time arrays, high resolution fluxgate magnetometer magnetic field arrays, and its corresponding time arrays.

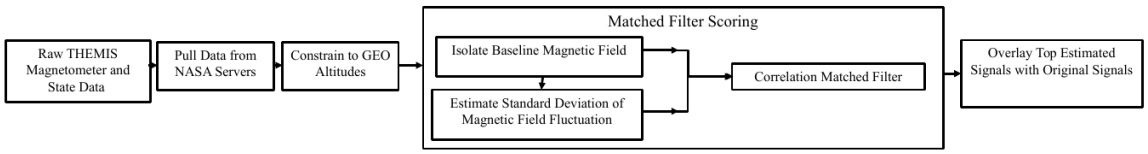

Figure 9. THEMIS Data Mining Process Diagram

The magnetometer data that satisfies the orbital constraint is then passed through the matched filter scoring process. This includes the low pass filtering, standard deviation estimation, and correlation scoring at each ω_m of interest. For a given section of data, if the maxima of the matched filter exceed a set threshold (typically SNR > 2), then the output file is appended with the primary parameters describing the signature and matched filter results. These parameters include:

- the THEMIS spacecraft (A-E) that measured the signature of interest
- the Unix time (epoch seconds since January 1, 1970 UTC) of the maximum magnitude of the signature of interest corresponding to the time at which the hypothesized RSO would reach its closest approach distance to the magnetometer (t_c)
- the estimate of the standard deviation (σ) of the filtered magnetic field of the at the time of closest approach
- the estimated maximum instantaneous apparent angular rate (ω_m) of the hypothesized RSO flyby
- the score of the matched filter process corresponding to the estimate of the local SNR of the signature of interest

The first two parameters listed are required for retrieval of the state and magnetometer signals while the final three parameters fully describe the estimated magnetic signature due solely to the hypothesized RSO. All of the parameters form the minimal set to represent the magnetic signature of a potential charged RSO encounter.

The final component of the THEMIS magnetometer data processing is to overlay the estimated signal from the scoring process output parameters on the raw signal, e.g. Figure 13. The estimated signal can be recreated using the estimated SNR of the signature, the local magnetic field standard variation, and the estimated angular rate (ω_m) of the signature. With the significantly reduced dataset, visual inspection of the scoring process results is performed on the resulting plots. This component of the data mining process is critical in identifying signatures that are characteristic of charged RSO flyby encounters and distinguishing these signatures from magnetosphere phenomenon.

Python was used as the programming language for this work due to the built-in and external open-source modules designed for FTP file retrieval and CDF extraction. Python is also advantageous in terms of computation speed and simple terminal interface for use on the GT PACE clusters.

Results

The results of the data mining process are shown in Table 1. For each THEMIS spacecraft, this table lists the number of magnetic signatures that are characteristic of charged RSO encounters. The matched filter detection counts are given under the MF column. These matched filter detections were then reduced to the Human Plausible detections through visual inspection of the estimated signal overlays. In early 2010, THEMIS-B and THEMIS-C branched into the ARTEMIS mission. From this point, the fluxgate magnetometer data was neglected from these spacecraft. Over the primary years of the THEMIS mission, there were no plausible detections from these two spacecraft. This is attributed to the high apogees of THEMIS-B and THEMIS-C, about 190,000 and 128,000 km respectively. Due to the large semi-major axis, these spacecraft spend a relatively small amount of time within the GEO altitude range of interest. Alternatively, the A, D, and E THEMIS spacecraft maintained lower apogee ranging from about 64,000 to 83,000 km. These spacecraft spend more time in or near GEO altitudes and have a higher probability of encountering a RSO. It should also be noted these lower apogee spacecraft also experience a larger number of GEO altitude magnetosphere phenomenon, resulting in a large amount of false detections by the matched filter scoring.

Table 1. Matched Filter and Human Plausible Detection Count, MF = Matched Filter, H = Human Plausible

S/C	THEMIS - A		THEMIS - B		THEMIS - C		THEMIS - D		THEMIS - E	
Year	**MF**	**H**	**MF**	**H**	**MF**	**H**	**MF**	**H**	**MF**	**H**
2007	0	0	0	0	0	0	0	0	0	0
2008	9	3	1	0	1	0	9	1	4	2
2009	4	1	0	0	0	0	7	2	5	2
2010	12	3	-	-	-	-	26	5	11	4
2011	14	3	-	-	-	-	30	4	6	1
2012	21	2	-	-	-	-	30	3	24	1
2013	0	0	-	-	-	-	41	6	59	6
2014	0	0	-	-	-	-	40	2	48	1
2015	0	0	-	-	-	-	23	2	20	1
2016	0	0	-	-	-	-	0	0	0	0
Total	60	12	1	0	1	0	206	25	177	18

From the analyzed dataset, a particular case of interest is the magnetometer signal from the THEMIS-A spacecraft with a UTC epoch time of 10-Aug-11 12:02:21. This case demonstrates the capability of the matched filter scoring process in detecting magnetic field signatures characteristic of the induced magnetic field signature of a RSO flyby. The following figures will detail the scoring process results on this particular dataset.

Following the process diagram outlined in Figure 9, the trend signal at the given ω_m is extracted using a zero phase low pass filter. In the case shown in Figure 10, the highest scored ω_m = 1.584 rad/s from the scoring process is used to calculate the cut-off frequency of the filter. As a result, the residual signal is a zero-mean signal that represents fluctuations over the baseline magnetic field.

At larger ω_m values of the scoring process, the low pass filter would instead attenuate this peak in the magnetic field magnitude and lower estimates of SNR will result at these ω_m values.

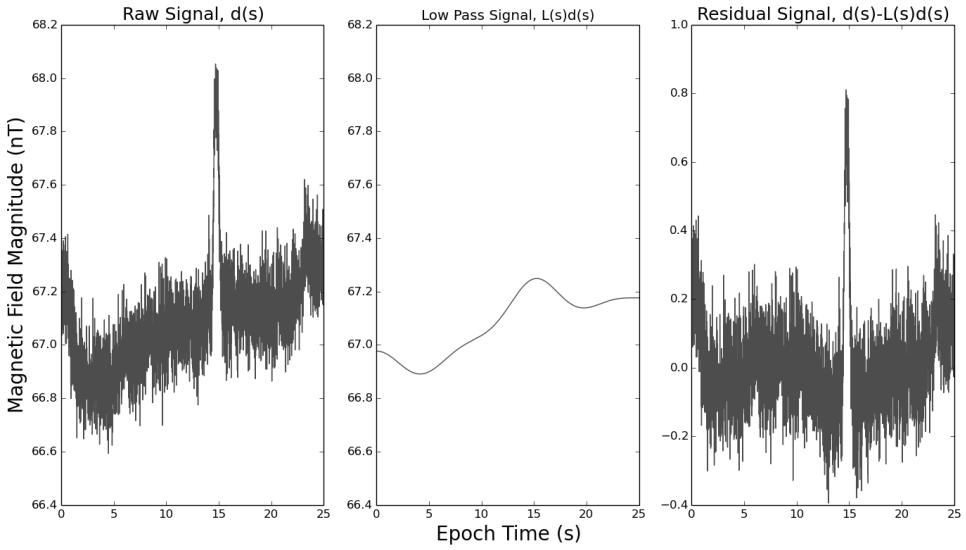

Figure 10. Low Pass Filter on THEMIS-A Dataset (at highest score ω_m=1.584 rad/s)

After performing a matched filter through time at multiple ω_m, a 3-dimensional surface of SNR estimates is created, with results shown in both Figure 11 and Figure 12. The coordinate location of the peaks of scoring surface estimate both the time at which a potential RSO flybys occurs as well as the relative angular rates between the RSO and the magnetometer. For this particular dataset, the estimated SNR of the signature is approximately 2.835, the estimated angular rate is 1.584 rad/s, and the UTC time of closest approach of 10-Aug-11 12:02:36.

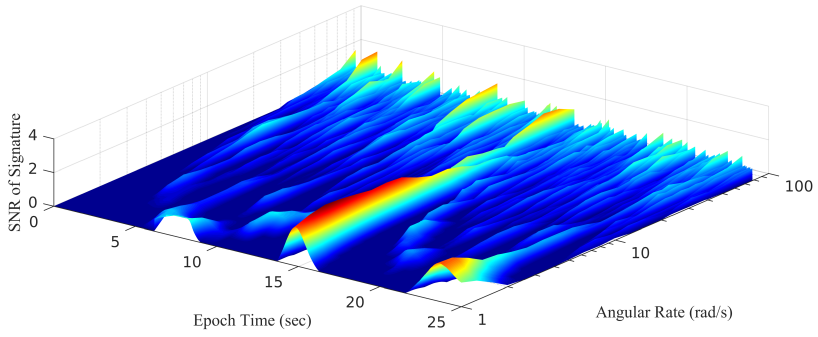

Figure 11. Scoring Surface for THEMIS-A Dataset

From the estimates generated from the scoring surface maxima, an artificial estimate signal is generated. When this artificial estimate signal is plotted with the true raw magnetometer signal, as in Figure 13, false detections or potential RSO signatures can be identified. The raw THEMIS fluxgate magnetometer signal is often erratic and includes many discontinuities in the magnetic field

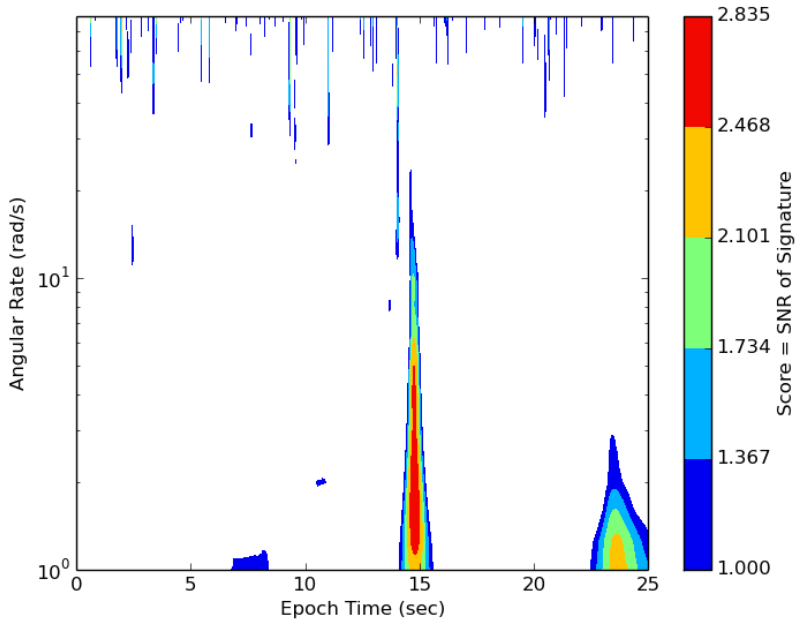

Figure 12. Scoring Contour for THEMIS-A Dataset

(at times on the order of tens of nanotesla). This can be attributed to THEMIS fluxgate magnetometers triggering high resolution data collection during magnetosphere phenomenon. Magnetospheric phenomenon, such as bow shock crossings and geomagnetic pulsations, can create peaks and discontinuous jumps in the magnetic field magnitude. Extraneous signals like this makes it more difficult for the scoring algorithm to distinguish and identify a characteristic signature of a RSO flyby. As a result, when visually inspecting the estimate signal overlay, the estimated signal must be relatively isolated from other large variations in the local magnetic field.

Visually, and in terms of the estimate parameters, the THEMIS-A dataset being discussed has a signature that is characteristic of a RSO encounter. To continue to support this hypothesis, an admissible region is formed to further constrain the possible states of the RSO. It is common to constrain detected space objects to have a negative orbital energy - relating to a closed Earth orbit. Holzinger showed the boundary of the admissible region constrained by maximum mass-specific energy may be found by computing the roots of a 7th order polynomial in $\rho_\perp$.[8] Using this, the potential orbits that satisfy the angular rate (ω_m) from the scoring algorithm and the closed orbit constraint can be plotted as shown in Figure 14. Figure 15 shows how the orbit solution space reduces when the solution set is limited to GEO altitude range.

Both the detection and elliptical orbit constraints are plotted in Figure 16. In this figure the light gray regions satisfy one of the constraints and the darker region, the joint admissible region, satisfies all constraints. For this particular case, the closed orbit constraint volume completely encompasses the detection constraint volume; the joint constraint volume may then be reduced to the detection constraint volume.

From Eq. (3) the possible vacuum charge can be found as a function of closest approach distance, $\rho_\perp$, given the estimated SNR and ω_m from the scoring process maxima. After assuming a $\bar{\lambda_d}$, it is

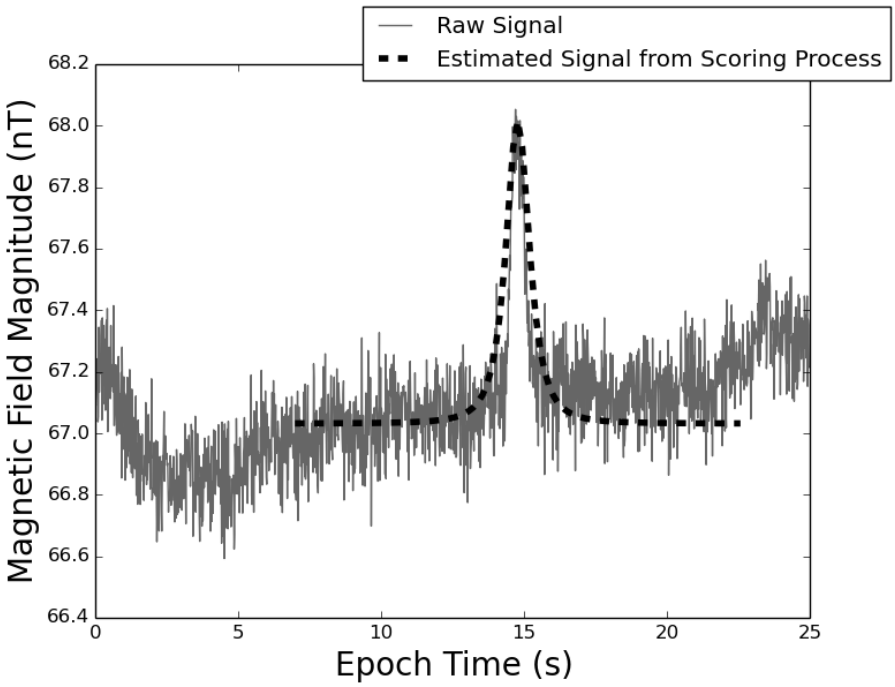

Figure 13. Matched Filter Estimate Over Raw THEMIS-A Signal

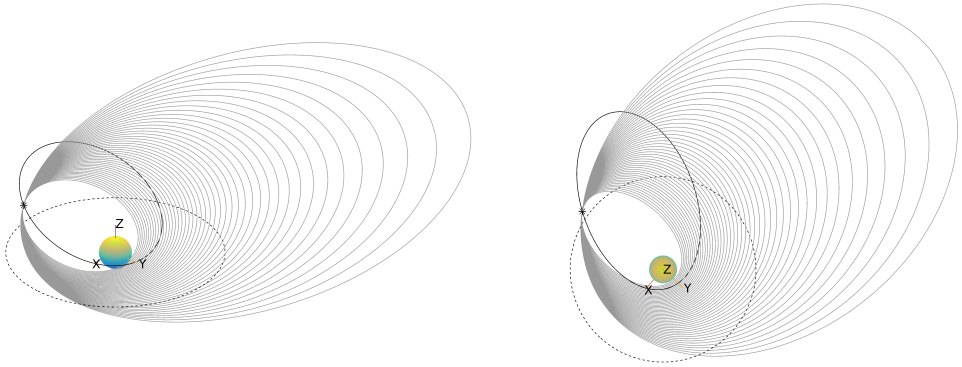

(a) Isometric View

(b) Top View ($\hat{\mathbf{i}} - \hat{\mathbf{j}}$ plane)

Figure 14. Closed Orbit Solutions to Admissible Region for THEMIS-A Dataset

possible to create a curve as shown in Figure 17. As a result of range limitations on both closest approach distance and vacuum charge, there is a limited solution space for plausible RSO flyby signatures. Graphically, only charge and distance solutions that lie within the unshaded region are possible for the expected RSO signatures. As a result, the hypothesized RSO flyby for this particular THEMIS-A dataset would occur within a closest approach distance of about 185 m.

The bounds of the admissible region can be further reduced by enforcing additional constraints on the vacuum charge, effective Debye length, and closest approach distance of the hypothesized RSO. As the effective Debye length, $\bar{\lambda}_d$, is decreased, the slope of the charge distance curve increases.

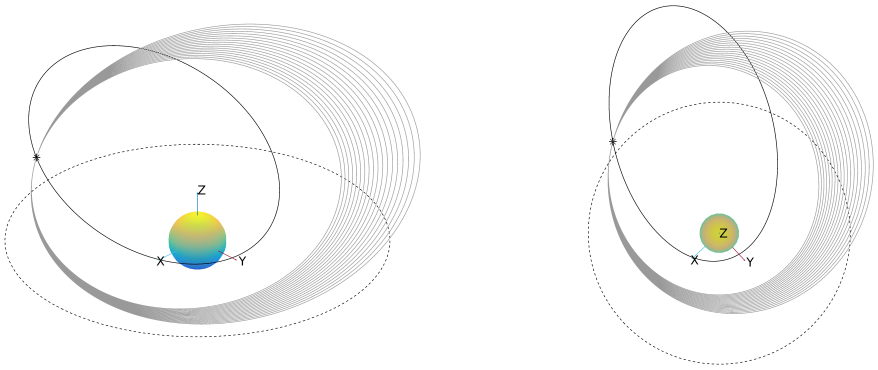

(a) Isometric View (b) Top View ($\hat{\mathbf{i}} - \hat{\mathbf{j}}$ plane)

Figure 15. GEO altitude Orbit Solutions to Admissible Region for THEMIS-A Dataset

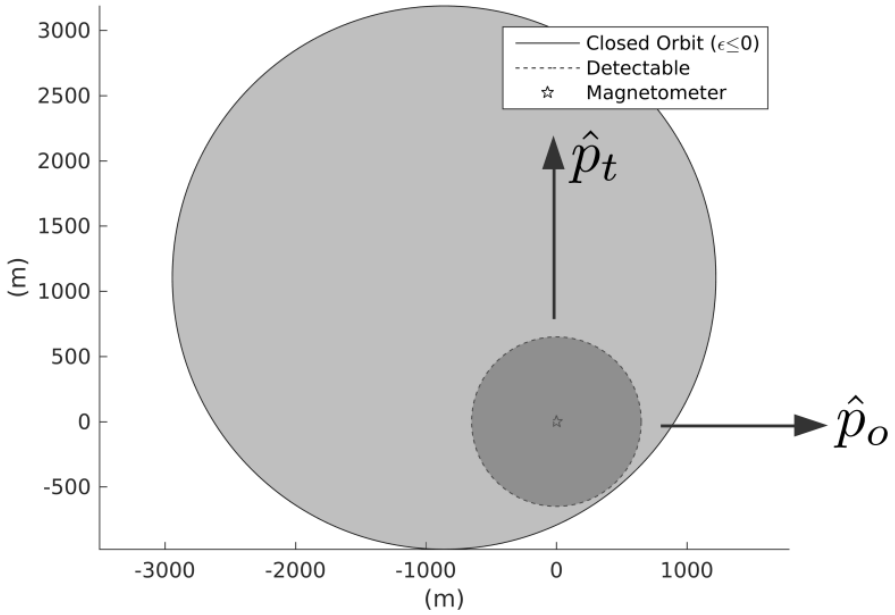

Figure 16. Admissible Region Constraints in Encounter Plane for THEMIS-A Dataset

However, due to the exponential scale of the Debye length, decreasing the effective Debye length from a maximal value of $\bar{\lambda}_d = 1000$ m to a nominal value of $\bar{\lambda}_d = 200$ m decreases the possible closest approach range from 185 m to 148 m (20% reduction). Additionally, the ratio $\sigma\text{SNR}/\omega_m$ is proportional to the slope of the charge distance curve. As a result, there is an upper limit of $\sigma\text{SNR}/\omega_m$ defined by the maximum possible vacuum charge, the minimum closest approach distance, and the effective Debye length. The upper limit of $\sigma\text{SNR}/\omega_m$ can be calculated analytically by rearranging Eq. (3). This upper limit of this ratio enforces an additional constraint on the SNR of the hypothesized RSO encounter. Graphically, this creates an upper boundary surface for scoring surfaces similar to Figure 11.

The total data analysis performed on the 128 Hz THEMIS magnetometer data resulted in 26 sig-

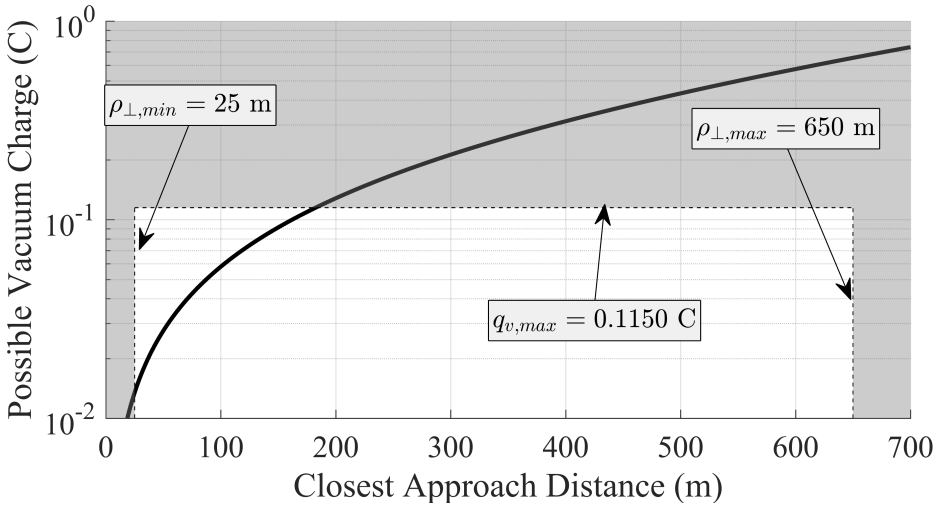

Figure 17. Potential Static Charge with varying Closest Approach Distance for THEMIS-A Dataset ($\bar{\lambda}_d$ = 1000 m)

natures that from the spacecraft constellation that were characteristic of the magnetic field generated from a charged RSO flyby. Figure 18 and Figure 19 briefly display the scoring results from two of these signatures of interest.

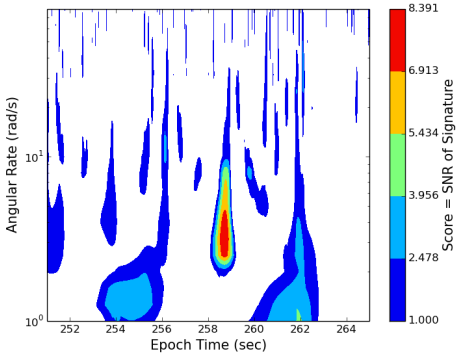

(a) Scoring Contour (SNR Estimate = 8.391)

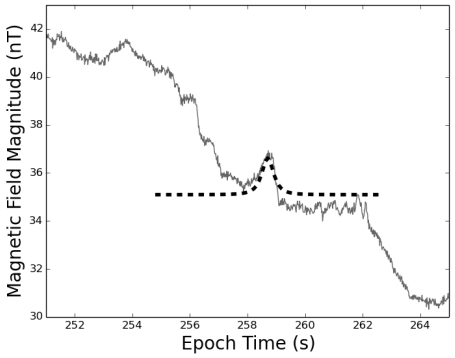

(b) Estimate Signal Overlay (ω_m Estimate = 3.158 rad/s)

Figure 18. THEMIS-E Scoring Algorithm Results from UTC epoch time on Monday, 10-May-10 13:24:57

FUTURE WORK

There are a number of detected signatures from the outlined data analysis. However, there is still work to be done to further analyze the detected signals as well as update the scoring algorithm. To further investigate the characteristics of the detected signatures, the data from each of the three magnetometer axes will be used to acquire the partial state information of the RSO. Furthermore, a more rigorous and constrained admissible region approach must constructed to constrain the subspace of

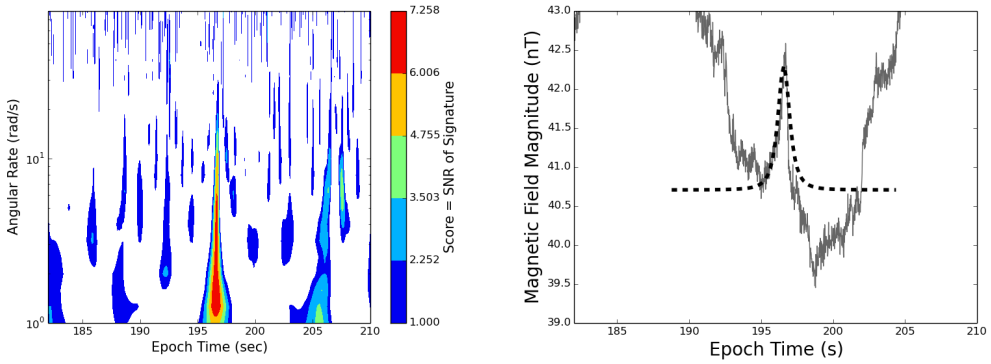

(a) Scoring Contour (SNR Estimate = 7.258)

(b) Estimate Signal Overlay (ω_m Estimate = 1.584 rad/s)

Figure 19. THEMIS-D Scoring Algorithm Results from UTC epoch time on Monday, 10-May-10 13:30:00

the unobservable parameters and give better estimates of the RSO orbital state.[9] The scoring process results will also be tested as a likelihood measurement using Binary Hypothesis testing.

For the scoring algorithm, beneficial updates include altering the filtering scheme. A bandpass filter can be implemented in lieu of a low pass filter. This update should extend the searchable range of ω_m, refine the autonomous filtering of magnetosphere phenomenon, and improve the frequency estimation of the scoring process. Debye length and charge screening effects will be incorporated to the scoring process, which should result in improved estimates of the signature SNR and ω_m.[6]

The THEMIS fluxgate magnetometer provides data at high sampling rates of 128 Hz, but this comes at the cost of erratic and unpredictable magnetic field signals of magnetosphere phenomenon. Additionally, a large number of the observed signatures of interest occur at lower angular rates, ω_m. As a result the lower sampling rate data from the THEMIS spacecraft will be analyzed using the scoring process. This dataset includes much larger data availability sets as well as calmer and more continuous magnetic field measurements.

CONCLUSIONS

In this paper, another phenomenology to detect RSOs at GEO altitudes is investigated. Starting from first principles, matched filtering techniques and signal processing have been used to examine the feasibility of using magnetometers to detect RSOs. The matched filter template is proposed and is consistent with the Biot Savart Law and approximate flyby dynamics. The detection capability of the THEMIS fluxgate magnetometers are discussed. To isolate local fluctuations in the baseline magnetic field, filtering and other signal conditioning options for raw magnetometer signals are introduced. The matched filter scoring process is presented and the results provide evidence of magnetic signatures that are characteristic of RSO flybys. Additional constraints are imposed on the signatures of interest using admissible regions and the presented plausible ranges of parameters that describe the signature.

REFERENCES

[1] "National Space Policy of the United States of America," tech. rep., June 2010.

[2] "The Space Report 2011," tech. rep., Space Foundation, Colorado Springs, CO, 2011.

[3] "NASA Technology Roadmaps TA 5: Communications, Navigation, and Orbital Debris Tracking and Characterization Systems," tech. rep., July 2015.

[4] *Continuing Kepler's Quest: Assessing Air Force Space Command's Astrodynamics Standards*. Committee for the Assessment of the U.S. Air Forces Astrodynamic Standards, Aeronautics and Space Engineering Board, Division on Engineering and Physical Sciences, and National Research Council, 2012.

[5] K. A. Heather Cowardin, P. Seitzer *et al.*, "Observations of Titan IIIC Transtage Fragmentation Debris," *Advanced Maui Optical and Space Surveillance Technologies (AMOS) Conference*, doi:20140002763.

[6] C. R. Seubert, L. A. Stiles, and H. Schaub, "Effective Coulomb force modeling for spacecraft in Earth orbit plasmas," *Advances in Space Research*, Vol. 54, No. 2, 2014, doi:http://dx.doi.org/10.1016/j.asr.2014.04.005.

[7] A. D. C. S. K. Kinard, W. H. *et al.*, *Orbiting Meteoroid and Debris Counting Experiment*, Vol. 1 of *LDEF (Long Duration Exposure Facility): 69 Months in Space. Third Post-Retrieval Symposium*. 1995.

[8] M. J. Holzinger, "Using Magnetometers for Space Object Characterization in Space Situational Awareness Applications," *Journal of Guidance, Control, and Dynamics*, Vol. 37, Sep 2014, doi:10.2514/1.g000523.

[9] G. Tommei, A. Milani, and A. Rossi, "Orbit determination of space debris: admissible regions," *Celestial Mechanics and Dynamical Astronomy*, Vol. 97, No. 4, 2007, doi:10.1007/s10569-007-9065-x.

[10] P. S. Gural, J. A. Larsen, and A. E. Gleason, "Matched Filter Processing for Asteroid Detection," *The Astronomical Journal*, Vol. 130, No. 4, 2005, p. 1951.

[11] G. L. Turint, "An introduction to matched filters," 1960.

[12] B. Thide, *Electromagnetic Field Theory*. Uppsala, Sweden: Upsilon Books, 2nd ed., 2004.

[13] V. A. J. L. Burch, "The THEMIS Mission," doi:10.1007/978-0-387-89820-9.

[14] H. Auster, K. Glassmeier, *et al.*, "The THEMIS Fluxgate Magnetometer," *The THEMIS Mission* (J. Burch and V. Angelopoulos, eds.), pp. 235–264, Springer New York, 2009.

[15] T. Derrick, B. Bates, and J. Dufek, "Evaluation of time-series data sets using the Pearson product-moment correlation coefficient," *Medicine and science in sports and exercise*, Vol. 26, July 1994, pp. 919–928.

[16] H.-S. Choi, J. Lee, K.-S. Cho, *et al.*, "Analysis of GEO spacecraft anomalies: Space weather relationships," *Space Weather*, Vol. 9, No. 6, 2011. doi:10.1029/2010SW000597.

[17] C. L. M. J. C. Frueh, D. Ferguson, "Passive Electrostatic Charging of Near-Geosynchronous Space Debris HAMR Objects and its Effects on the Coupled Object Dynamics," *AAS/AIAA Spaceflight Mechanics Meeting*, 2014.

[18] R. M. Corless, G. H. Gonnet, D. E. G. Hare, *et al.*, "On the Lambert W Function," *Advances in Computational Mathemetics*, 1996, pp. 329–359.

[19] J. A. Ratcliffe, *An Introduction to the Ionosphere and Magnetosphere*. CUP Archive, 1972.

[20] S. M. P. A. Chulliat, A. *et al.*, "The US/UK World Magnetic Model for 2015-2020," tech. rep., doi:10.7289/V5TB14V7.

[21] C. Wang, J. B. Liu, Z. H. Huang, *et al.*, "Response of the magnetic field in the geosynchronous orbit to solar wind dynamic pressure pulses," *J. Geophys. Res.*, Vol. 112, doi:10.1029/2007ja012664.

[22] K. Heinz and D. Gubbins, *Geomagnetic Pulsations*. Encyclopedia of Geomagnetism and Paleomagnetism, encyclopedia of geomagnetism and paleomagnetism ed., 2007.

[23] K. L. Makovec, *A Nonlinear Magnetic Controller for Three-Axis Stability of Nanosatellites*. PhD thesis, Virginia Polytechnic Institute and State University, 2001.

[24] V. Angelopoulos, "The ARTEMIS Mission," *Space Science Reviews*, Vol. 165, No. 1-4, 2011, doi:10.1007/s11214-010-9687-2.